6.10.2009

The T-matrix method

Jani Tyynelä

History

- T-matrix method (TMM) is based on the extended boundary condition method (EBCM) by Waterman (1965-1979)
- Barber and Yeh (1975-1982) actually introduced the name EBCM and made the method more widely used
- the name '*T*-matrix formalism' was introduced by Ström (1975)
- in acoustic applications, TMM is known as 'the null-field method'
- Iskander *et al.* (1982-1984) introduced an iterative version of TMM to improve the convergence
- Mishchenko (1990-1994) proposed to use of extended precision in order to use TMM for higher size parameters, and also developed an efficient way to use analytical averaging over orientations to speed up computations
- superposition TMM was introduced by Mackowski and Mishchenko (1996) for a cluster of spheres

Basics

- TMM can be considered to be an extension of Mie theory to particles without spherical symmetry
- in TMM incident, scattered and internal fields are expanded in vector spherical harmonic functions
- the *T*-matrix itself transforms the incident field expansion coefficients to the scattered field expansion coefficients
- the main advantage of TMM over volume-based methods like DDA is an efficient use of symmetries, better accuracy, and analytical averaging over orientations

Computing the T-matrix

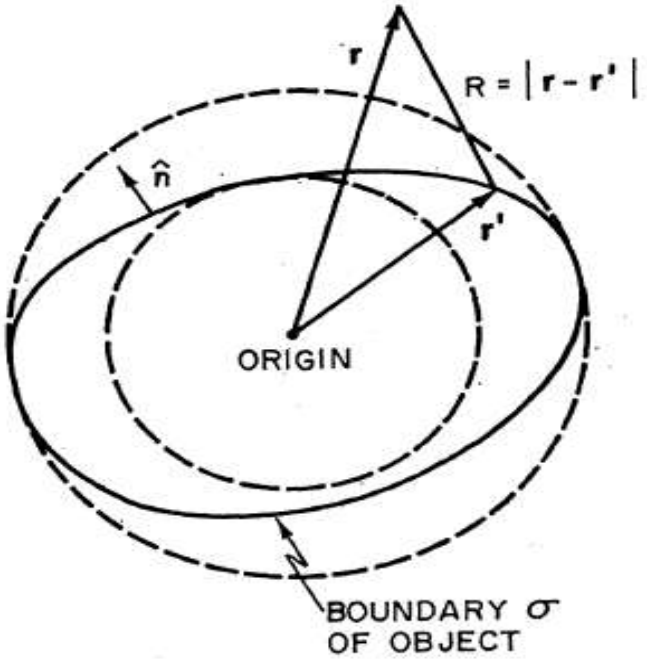

FIG. 1. Geometry of a scattering region bounded by the closed surface σ.

Computing the T-matrix

Huygens principle is used to establish a relationship between the total field and the incident field using the integral equation,

$$\begin{Bmatrix} \vec{E}_{tot}(\vec{r}) \\ 0 \end{Bmatrix} = \vec{E}_{inc}(\vec{r}) + \nabla \times \int_S (\vec{n} \times \vec{E}_{outside}) g(kR)\, dS - \frac{1}{i\omega\epsilon_0} \nabla \times \nabla \times \int_S (\vec{n} \times \vec{H}_{outside}) g(kR)\, dS, \vec{r} \begin{Bmatrix} outside\ \sigma \\ inside\ \sigma \end{Bmatrix}$$

where $g(kR) = \frac{e^{ikR}}{4\pi R}$ is the Green's function.

The surface integrals can be interpreted as surface currents that are the sources of the scattered field according to the equivalence theorem, but this also results in zero total field inside the scatterer. The object is to solve the surface integrals using the incident field expansion and the physical characteristics of the scatterer.

Computing the T-matrix

External problem:

1. Incident field is expanded in vector spherical harmonic functions

$$\vec{E}_{inc}(\vec{r}) = \sum_{n=1}^{N_{max}} \sum_{m=-n}^{n} [a_{mn} Rg\, \vec{M}_{mn}(k\vec{r}) + b_{mn} Rg\, \vec{N}_{mn}(k\vec{r})],$$

2. The surface integrals are also expanded and the surface currents $\vec{n} \times \vec{E}_{outside}$ and $\vec{n} \times \vec{H}_{outside}$ are solved using the incident field coefficients

$$\vec{E}_{inc} = -\int_S f(\vec{n} \times \vec{E}_{outside}, \vec{n} \times \vec{H}_{outside})\, dS$$

Computing the T-matrix

Internal problem:

3. The internal field is expanded

$$\vec{E}_{int}(\vec{r}) = \sum_{n=1}^{N_{max}} \sum_{m=-n}^{n} \left[c_{mn} \vec{M}_{mn}(mk\vec{r}) + d_{mn} \vec{N}_{mn}(mk\vec{r}) \right]$$

4. The tangential components $\vec{n} \times \vec{E}_{inside}$ and $\vec{n} \times \vec{H}_{inside}$ are solved using the internal field coefficients

5. Using boundary conditions $\vec{n} \times \vec{H}_{outside} = \vec{n} \times \vec{H}_{inside}$ and $\vec{n} \times \vec{E}_{outside} = \vec{n} \times \vec{E}_{inside}$ a relation between the incident and internal field coefficients is obtained

in matrix form:

$$\begin{bmatrix} a \\ b \end{bmatrix} = \begin{bmatrix} Q_{11} & Q_{12} \\ Q_{21} & Q_{22} \end{bmatrix} \begin{bmatrix} c \\ d \end{bmatrix}$$

Computing the T-matrix

Scattered field:

6. The scattered field is expanded

$$\vec{E}_{sca}(\vec{r}) = \sum_{n=1}^{N_{max}} \sum_{m=-n}^{n} [\, p_{mn} \vec{M}_{mn}(k\vec{r}) + q_{mn} \vec{N}_{mn}(k\vec{r}) \,], \; r > r_{sph}$$

7. Using the solved internal field coefficients, the tangential components $\vec{n} \times \vec{E}_{inside}$ and $\vec{n} \times \vec{H}_{inside}$ can be obtained, and the scattered field, when substituted into the integral equation

in matrix form:

$$\begin{bmatrix} p \\ q \end{bmatrix} = - \begin{bmatrix} Rg\,Q_{11} & Rg\,Q_{12} \\ Rg\,Q_{21} & Rg\,Q_{22} \end{bmatrix} \begin{bmatrix} c \\ d \end{bmatrix}$$

8. The *T*-matrix is:

$$T = -Rg\,Q\,Q^{-1}$$

Computing the T-matrix

- due to the singularity of Green's function, the expansion is only valid for the regions outside the circumscribing sphere ($r>r_{sph}$)
- according to Rayleigh hypothesis the expansion is valid, but this has never been proved
- Waterman (1971) proved that the expansion of the field is valid inside the whole boundary
- convex shape is not required in the TMM formulation (proved by Waterman, 1979)

Computing the T-matrix

- in practical applications, particle symmetries are used to enhance the computational speed and codes are used only on certain simple shapes like spheroids, finite circular cylinders etc.
- if the particle has a rotational symmetry with respect to the z-axis, all surface integrals reduce to single integrals over the polar angle, and the T-matrix becomes symmetric with respect to the m and m' indices
- the integrals can be easily evaluated with Gauss quadrature or the trapezium rule

Advantages of TMM

- computationally fast for rotationally symmetric particles, $O(N^6)$ for computing Q and RgQ matrices, DDA is $O(N^7)$
- exact solution for most non-spherical particles, applicable in size up to about x=100
- for particles with spherical symmetry is the same as Mie theory
- when the T-matrix of a particle in any orientation is known, it can be computed in any other orientation a lot faster than doing the T-matrix computations again
- T-matrix itself is a function of particle shape, size, refractive index, and orientation, but is independent on incident polarization and direction as well as the scattered direction
- orientation averaging can be done analytically using Euler angle rotations, and it can be about a factor of several tens faster than doing the numerical integration
- superposition TMM is rather straight-forward and maintains some of the advantages of normal TMM

Limitations of TMM

- for particles with no symmetry, TMM is generally not faster than other surface-integral methods like the generalized point matching method
- few available TMM codes for arbitrary shaped particles
- applicable only for homogeneous particles, but can be extended to a layered structure
- small errors in the Q-matrix can become large errors in Q^{-1}, these errors increase as size or aspect ratio is increased

TMM applications

- shapes that can be modeled with the available TMM codes:
  - spheroids
  - finite circular cylinders
  - Chebyshev-polynome shapes
  - finite polyhedral cylinders
  - cluster of spheres

TMM applications: spheroids

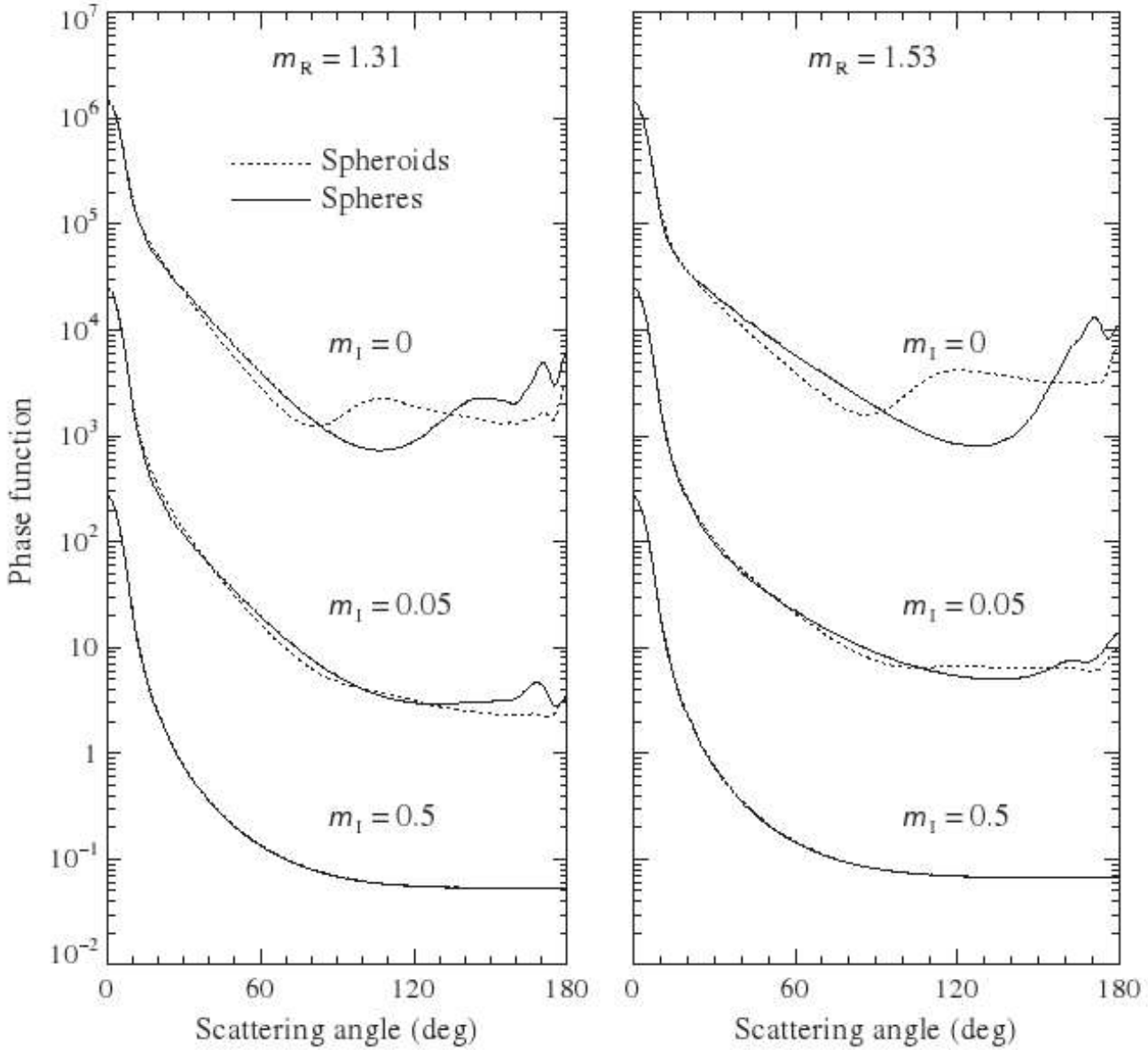

Figure 10.15. Phase function a_1 versus scattering angle Θ for polydisperse, randomly oriented oblate spheroids with an axis ratio 1.7 and for surface-equivalent spheres. The results are shown for two values of the real part of the relative refractive index ($m_R = 1.31$ and 1.53) and three values of the imaginary part ($m_I = 0$, 0.05, and 0.5). The size distribution is given by Eq. (5.246) with $\alpha = -3$ and $v_{eff} = 0.1$. The effective size parameter is $x_{eff} = 15$. The vertical axis scale applies to the curves with $m_I = 0.5$, the other curves being successively displaced upward by a factor of 100.

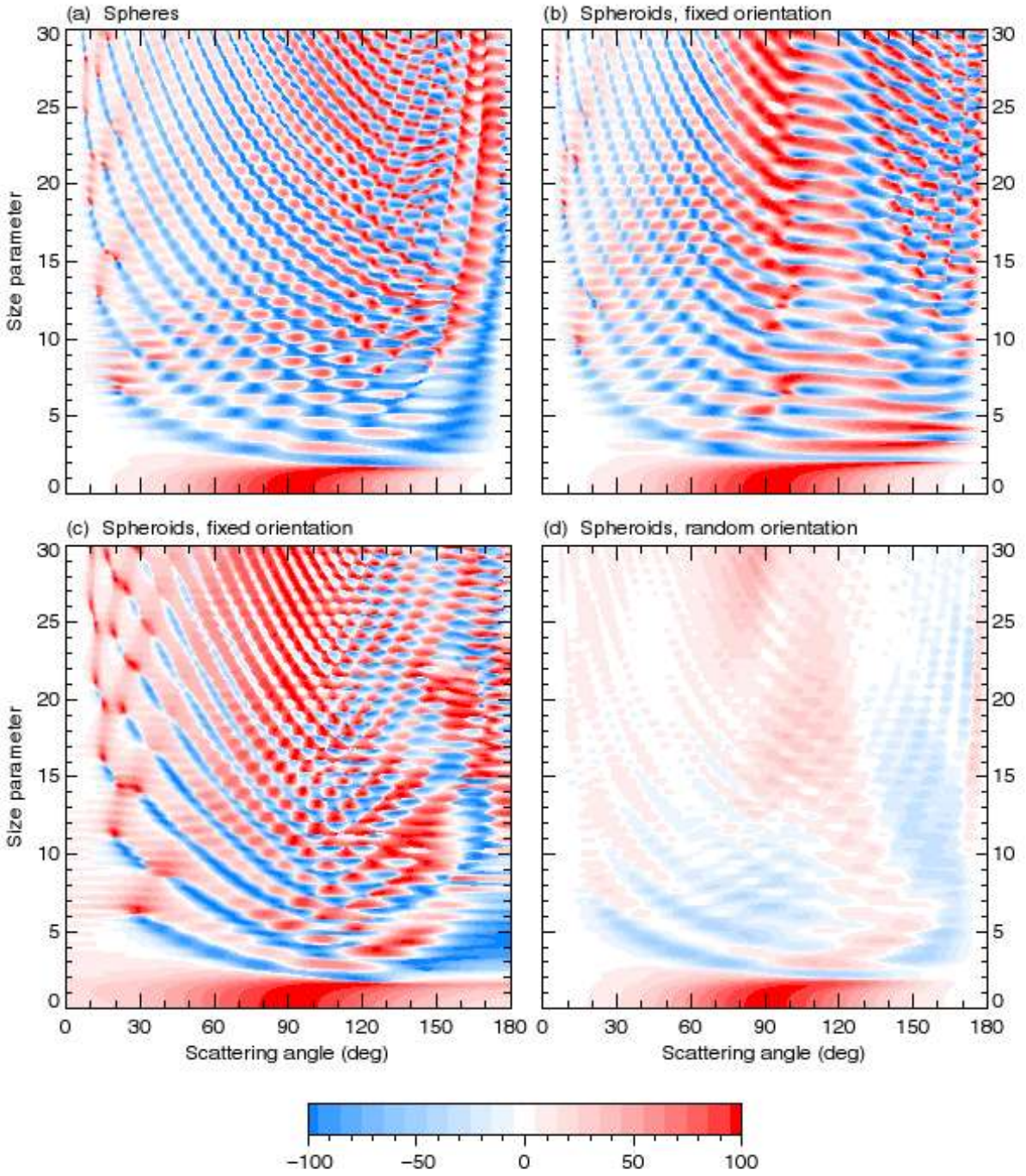

Plate 10.1. The ratio $-Z_{21}(\vartheta^{sca}, \varphi^{sca}=0; \vartheta^{inc}=0, \varphi^{inc}=0)/Z_{11}(\vartheta^{sca}, \varphi^{sca}=0; \vartheta^{inc}=0, \varphi^{inc}=0)$ in % versus ϑ^{sca} and size parameter for monodisperse spheres and surface-equivalent oblate spheroids in fixed and random orientations. In panels (b) and (c), the rotation axis of the spheroids is oriented respectively along the z-axis and along the x-axis of the laboratory reference frame. The relative refractive index is $1.53 + i0.008$ and the spheroid axis ratio $a/b = 1.7$.

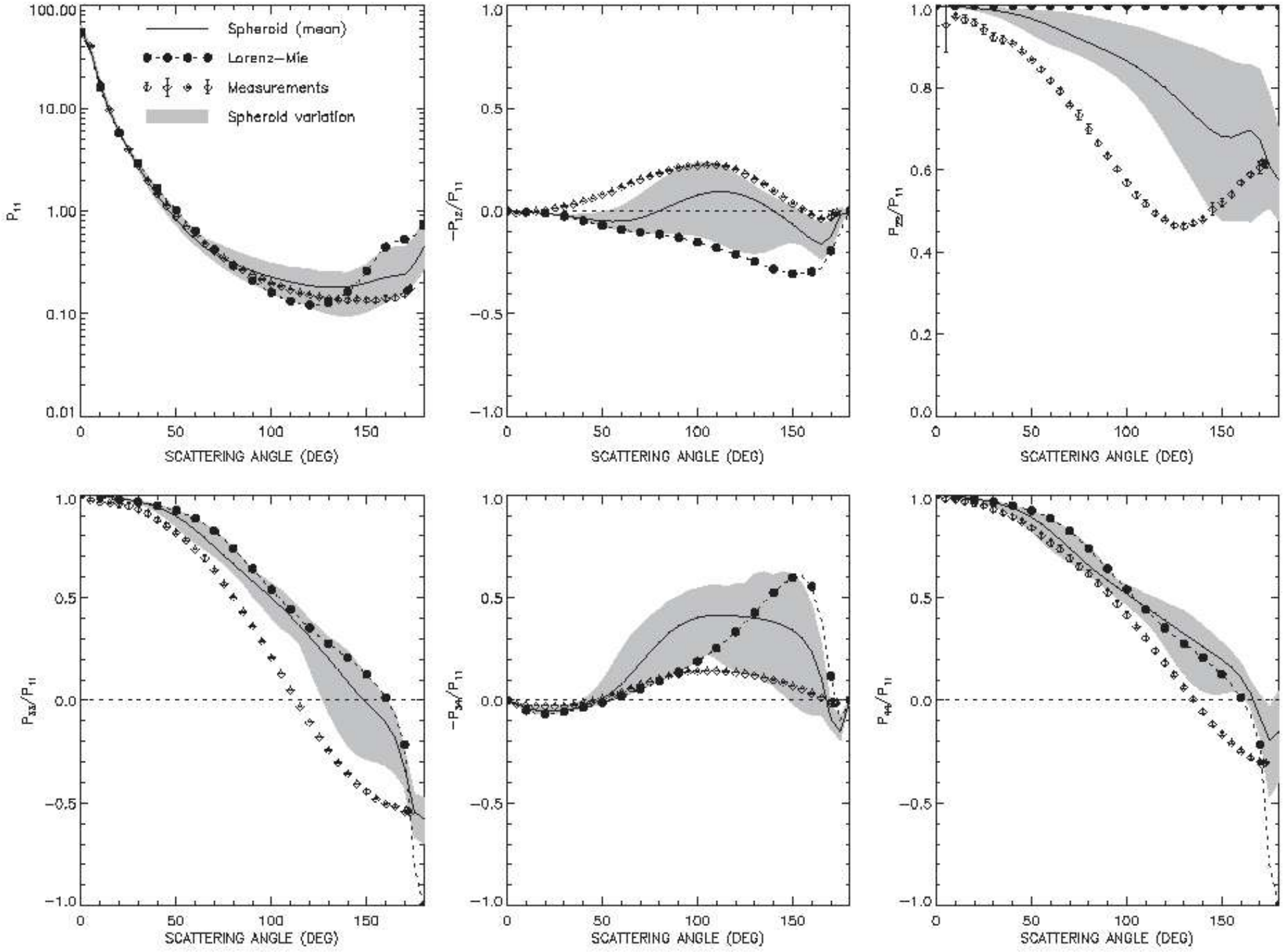

Fig. 3. Same as Fig. 2, except for equi-probable distribution of oblate spheroids.

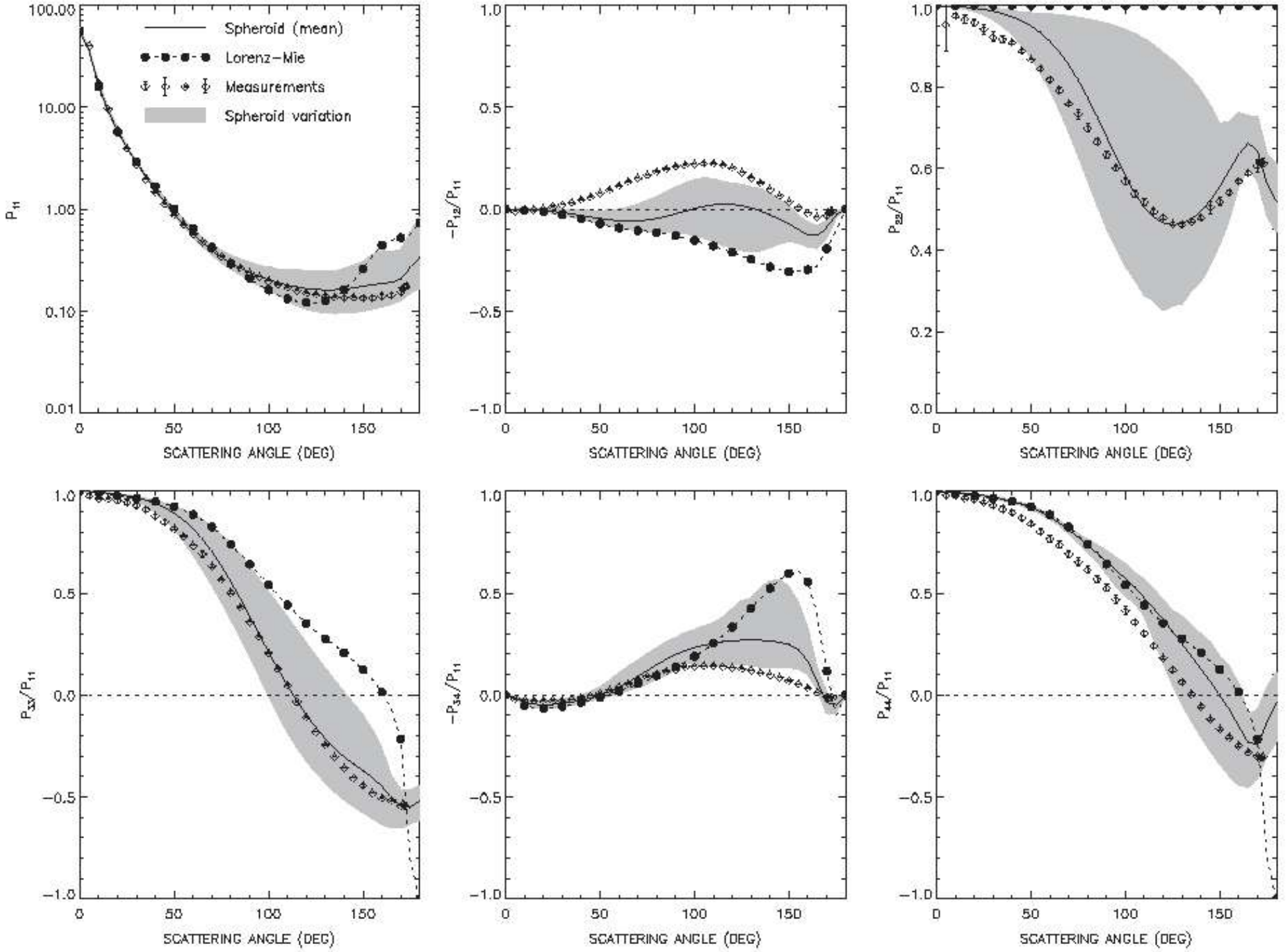

Fig. 4. Same as Fig. 2, except for equi-probable distribution of prolate spheroids.

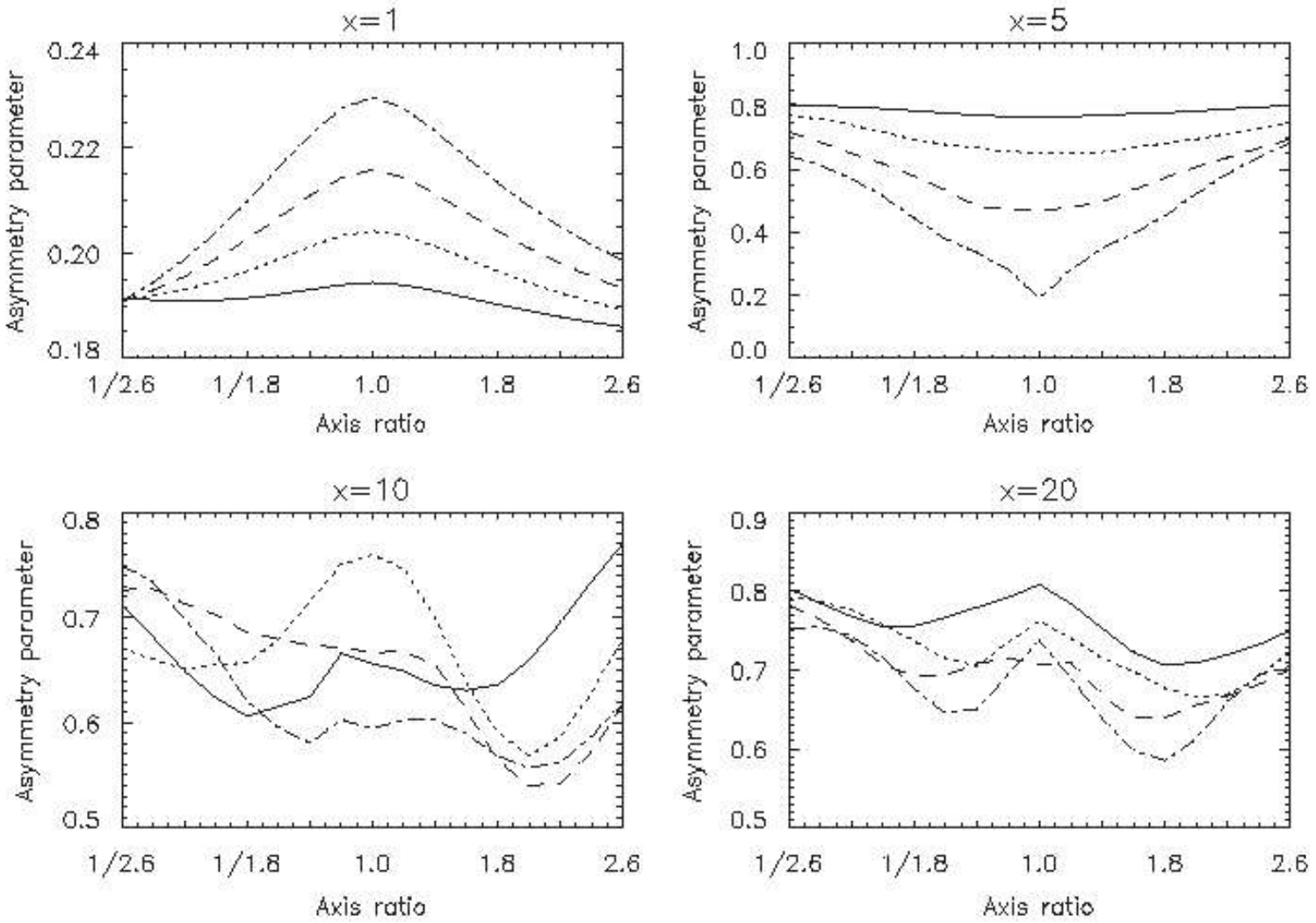

Fig. 2. As Fig. 1 but for Re(m) values of 1.45 (solid line), 1.55 (dotted line), 1.65 (dashed line), and 1.75 (dash-dotted line). Im(m) has been fixed to 0.001.

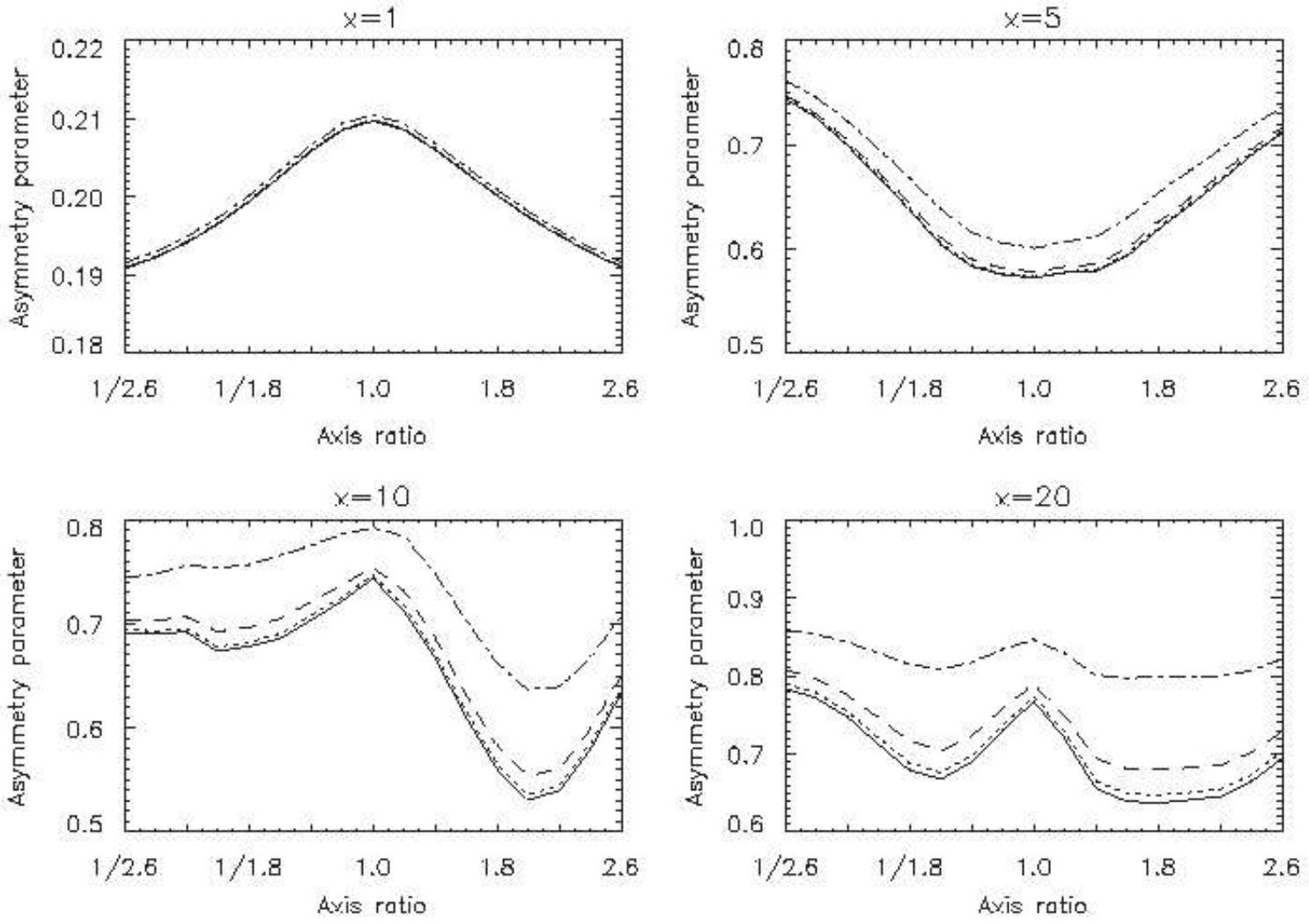

Fig. 1. The dependence of the asymmetry parameter g on the spheroid axis ratio. The panels show the results for size parameters 1, 5, 10, and 20. The different lines stand for Im(m) values of 0.0001 (solid line), 0.0005 (dotted line), 0.002 (dashed line), and 0.01 (dash-dotted line). Re(m) has been fixed to 1.6.

TMM applications: cylinders

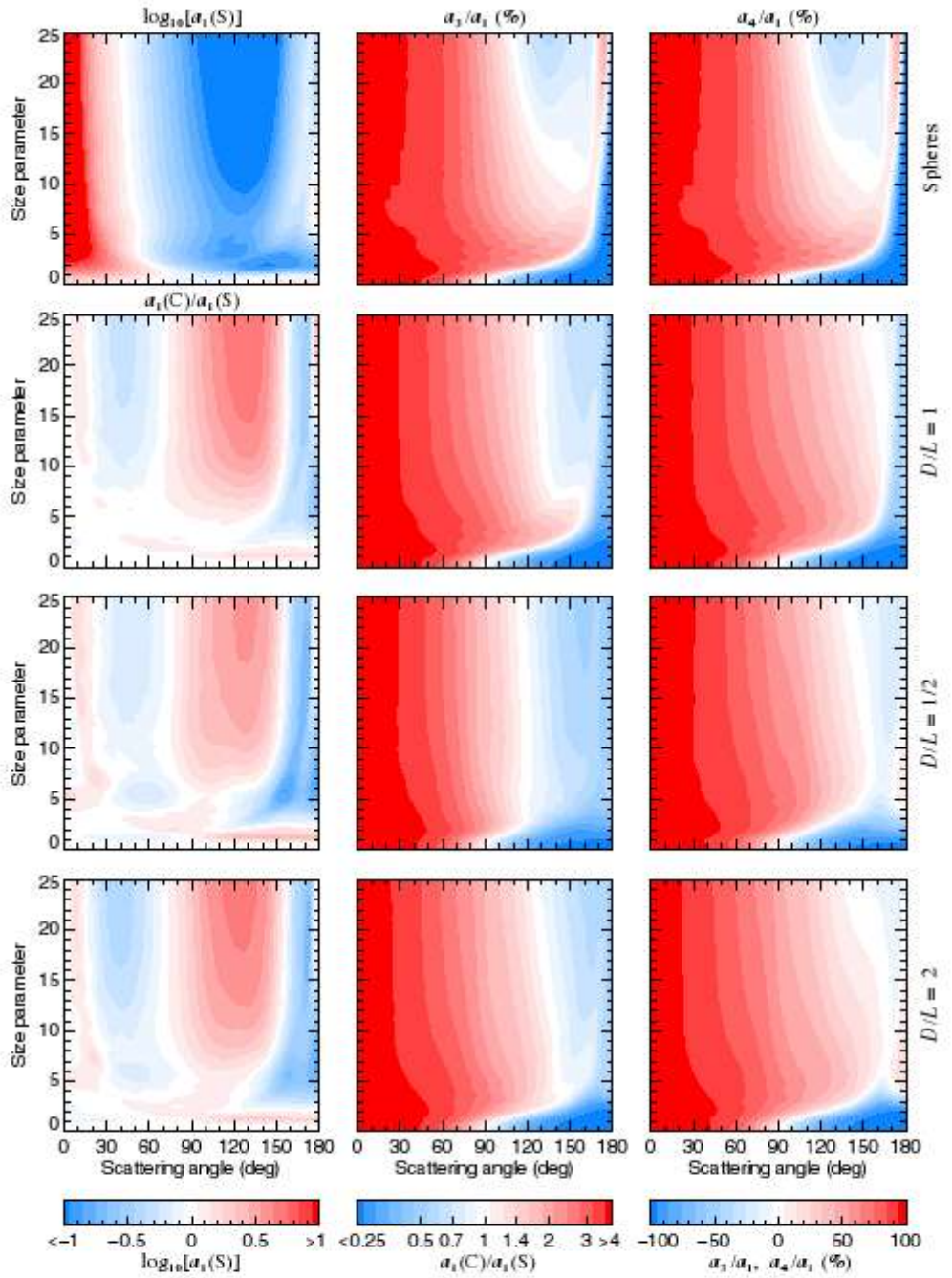

Plate 10.5. The top left panel shows the logarithm of the phase function versus scattering angle and effective size parameter for polydisperse spheres. The three lower diagrams in the left-hand column show the ratio of the phase function $a_1(C)$ for polydisperse randomly oriented cylinders with $D/L = 1, 1/2$, and 2 and the phase function $a_1(S)$ for surface-equivalent spheres. The middle and right-hand columns show a_3/a_1 and a_4/a_1 for spheres (top panels) and for surface-equivalent cylinders (lower three pairs of panels). Each diagram is quantified by the corresponding color bar at the bottom of the plate. All particles have the same relative refractive index, 1.53 + i0.008. The distribution of surface-equivalent-sphere radii is given by Eq. (5.246) with $\alpha = -3$ and $v_{\text{eff}} = 0.1$.

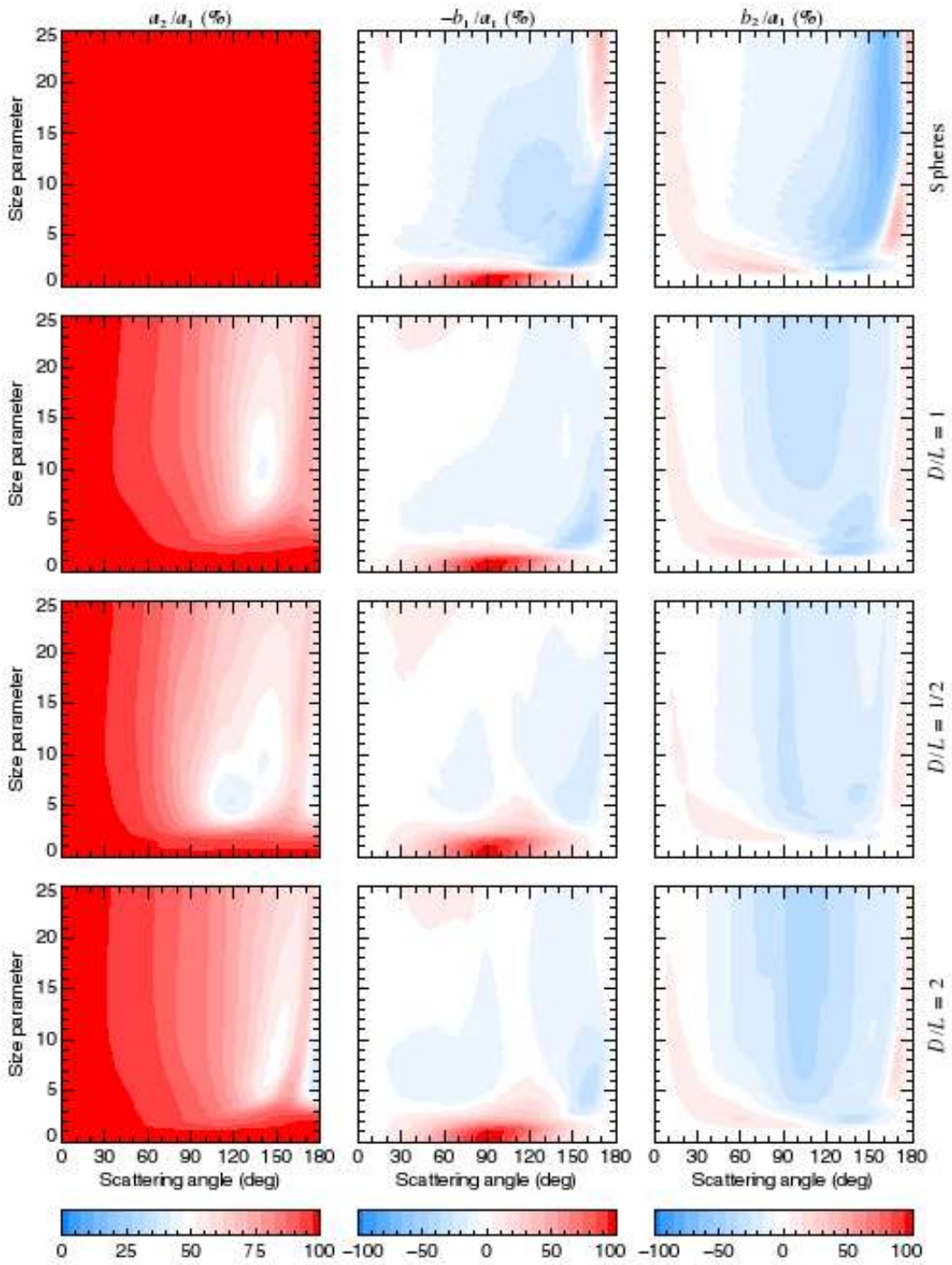

Plate 10.6. The ratios a_2/a_1, $-b_1/a_1$, and b_2/a_1 for polydisperse spheres and for surface-equivalent randomly oriented cylinders with $D/L = 1, 1/2$, and 2. The diagrams in each column are quantified using the color bar below the column. All particles have the same relative refractive index, 1.53 + i0.008. The distribution of surface-equivalent-sphere radii is given by Eq. (5.246) with $\alpha = -3$ and $v_{\text{eff}} = 0.1$.

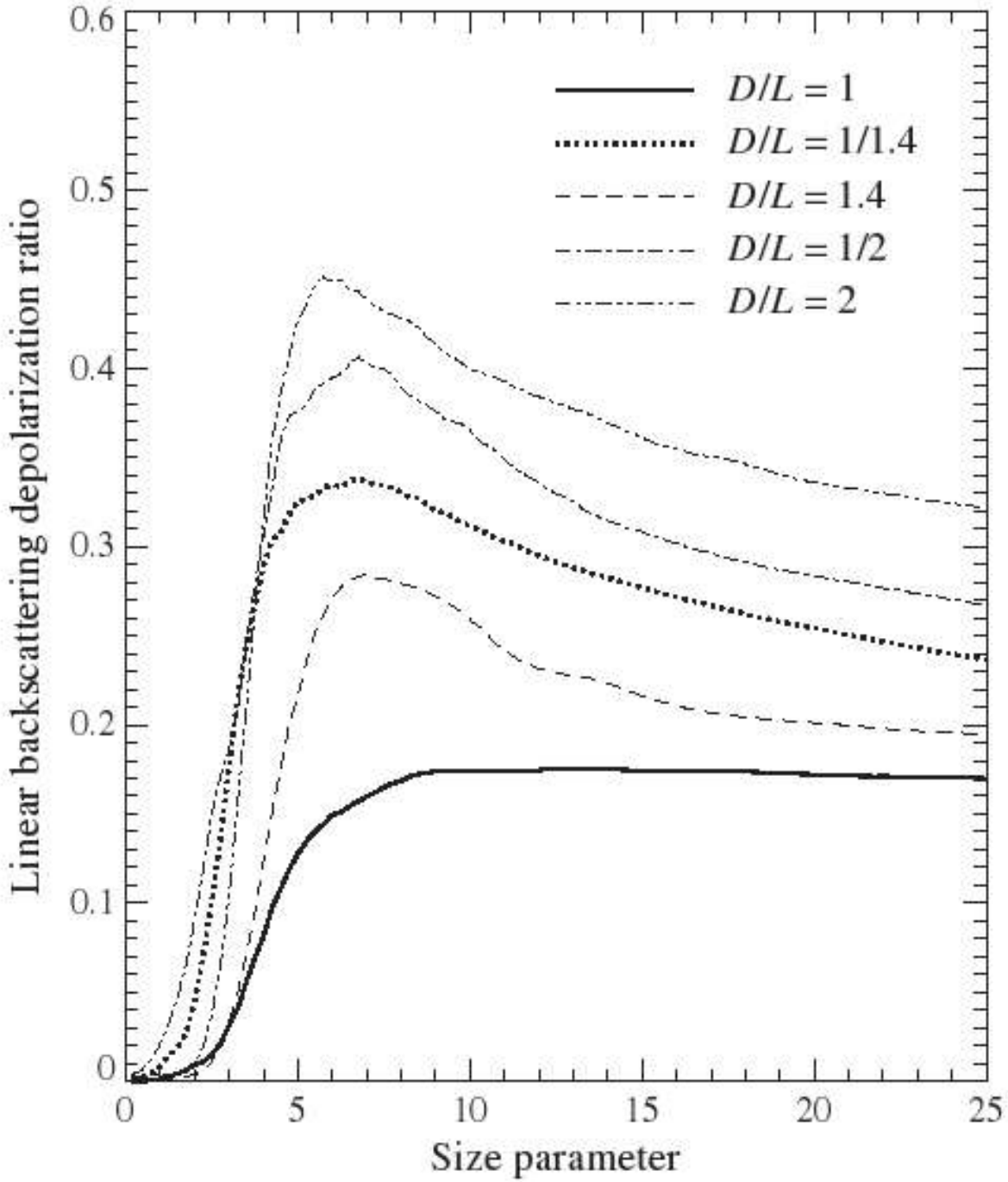

Figure 10.26. Linear backscattering depolarization ratio versus effective size parameter for randomly oriented polydisperse cylinders.

TMM applications: Chebyshev shapes

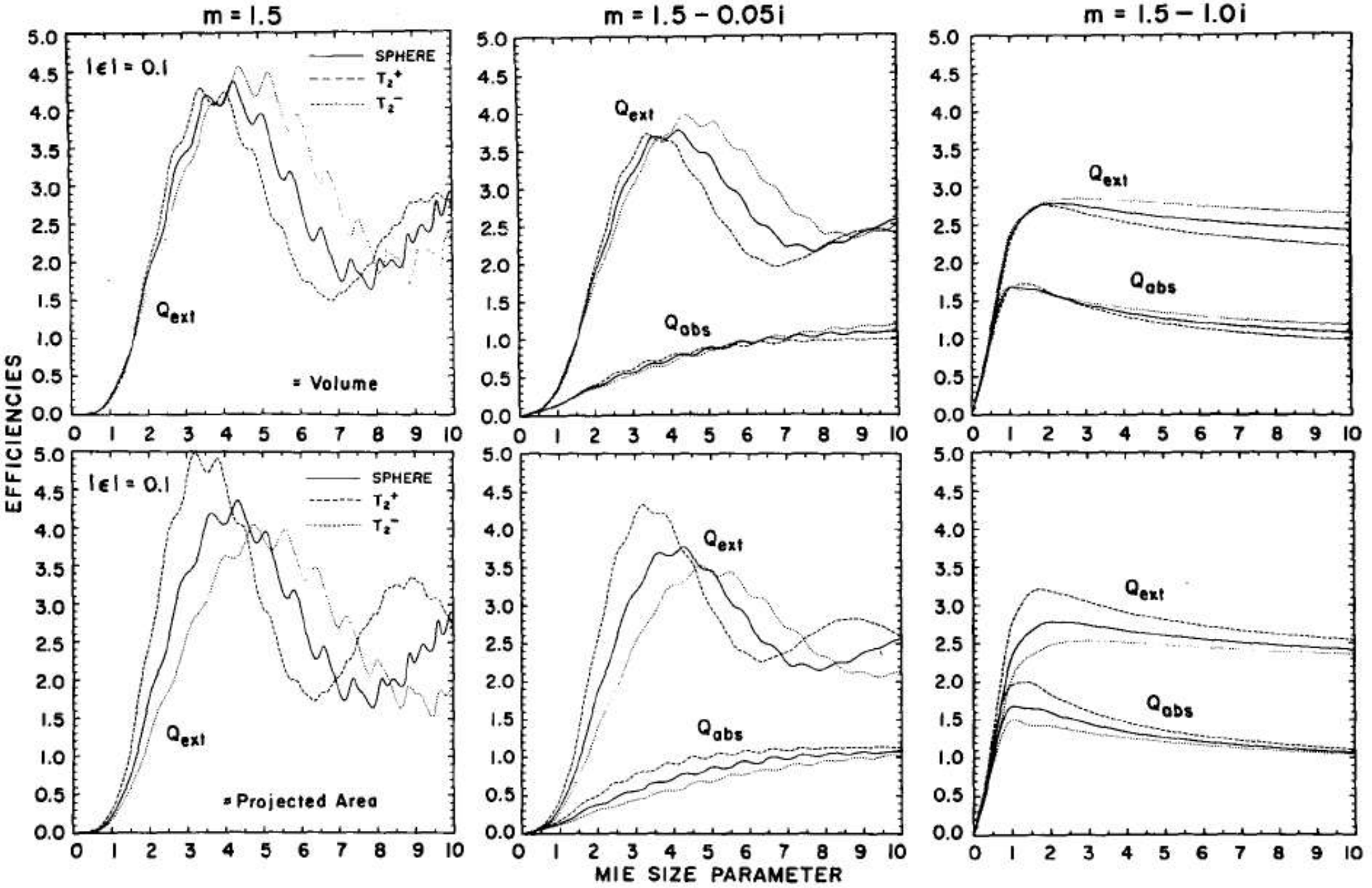

FIG. 3. Q_{ext} and Q_{abs} versus x_{ev} (top row) and versus x_{epa} (bottom row) for $T_2^{\pm}$ particles with $|\epsilon| = 0.1$ at nose-on incidence. Corresponding results for a sphere are also shown. Refractive indices of 1.5, $1.5 - 0.05\,i$, and $1.5 - i$ in the three columns, respectively.

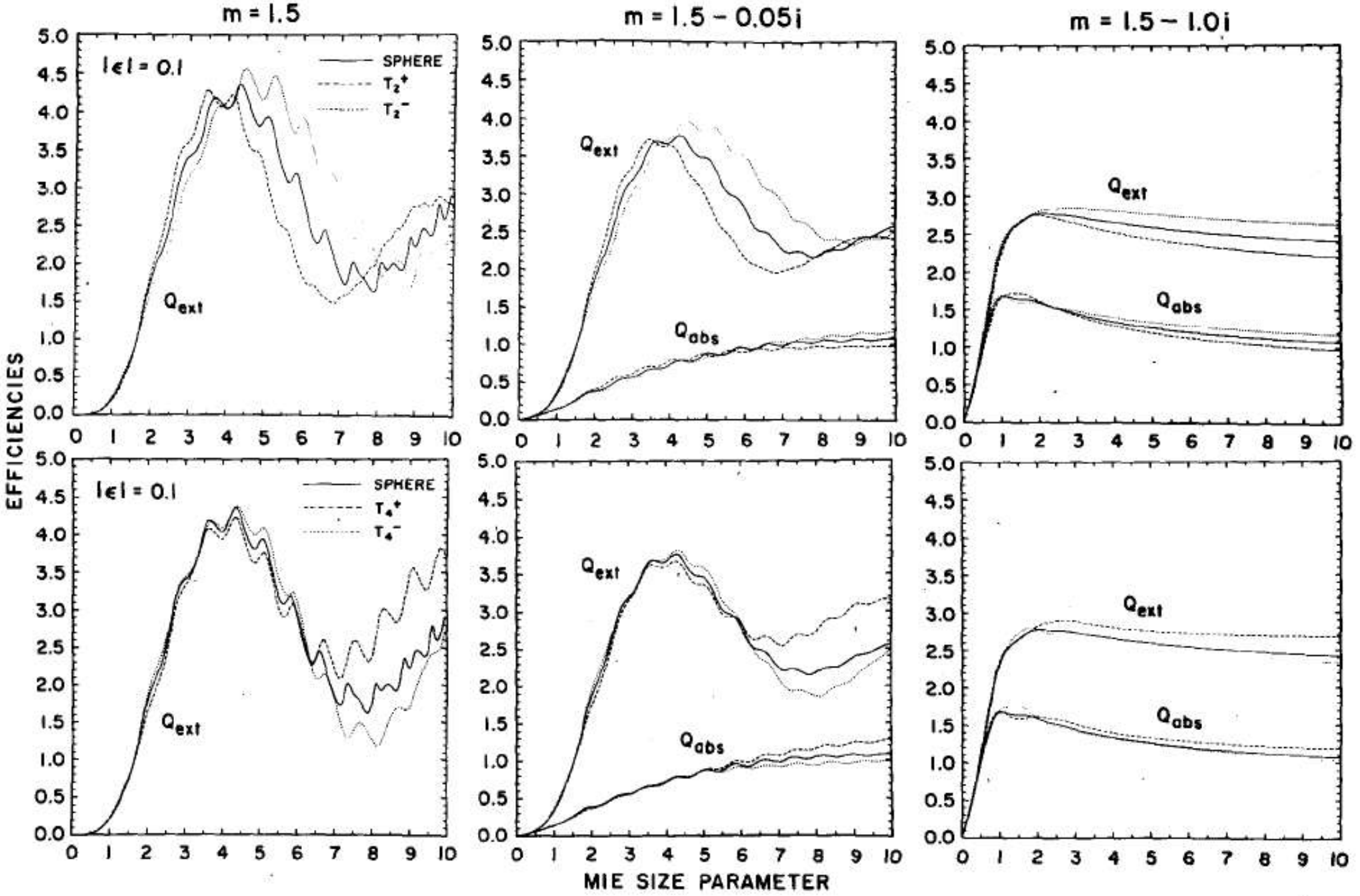

FIG. 4. Q_{ext} and Q_{abs} versus x_{ev} for $T_2^{\pm}$ (top row) and $T_4^{\pm}$ (bottom row) particles with $|\epsilon| = 0.1$ at nose-on incidence. Also corresponding spherical results.

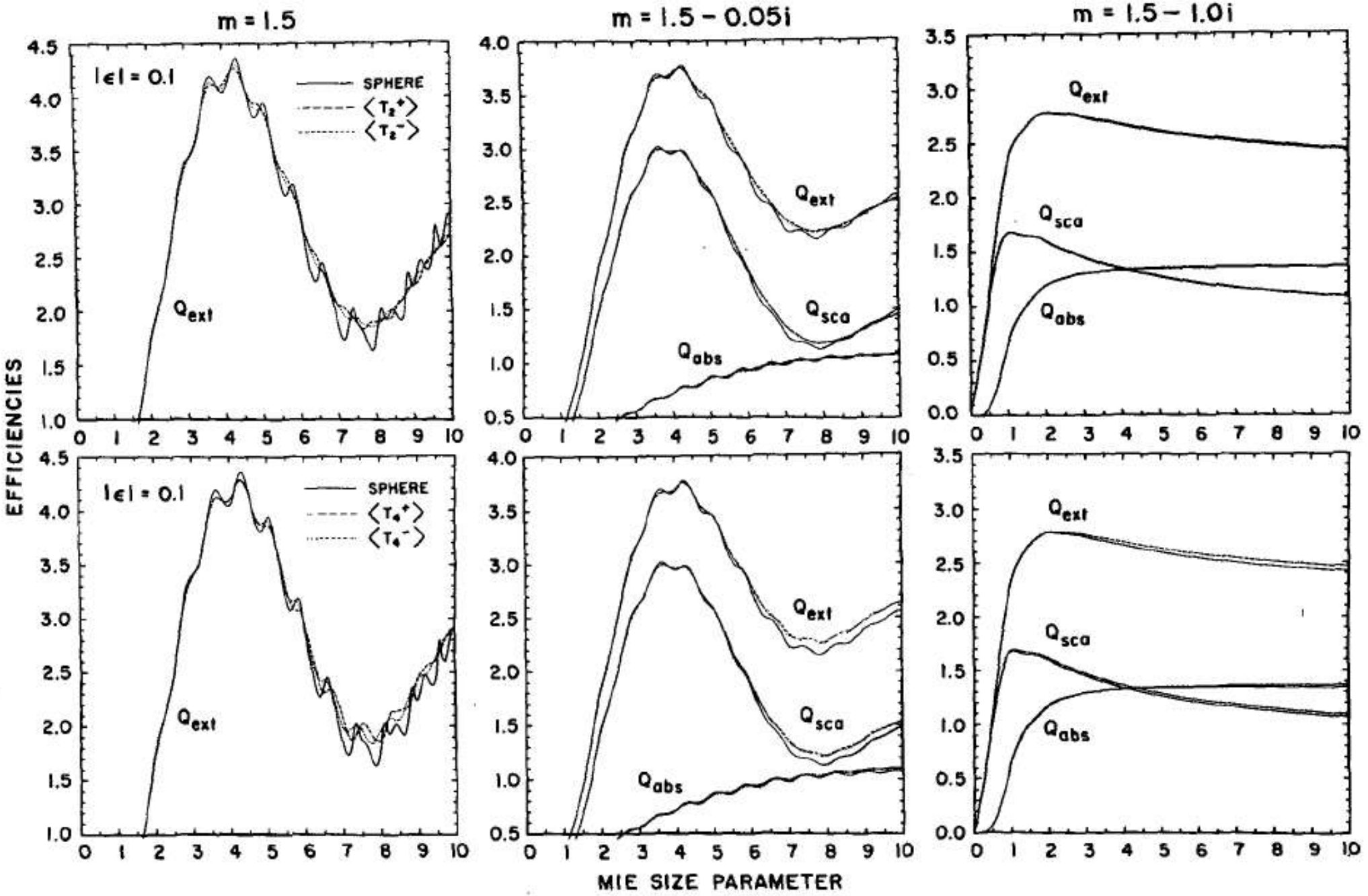

FIG. 5. Q_{ext} and Q_{abs} versus x_{ev} for randomly oriented $T_2^{\pm}$ (top row) and $T_4^{\pm}$ (bottom row) particles with $|\epsilon| = 0.1$. Also corresponding spherical results.

TMM applications: Prisms

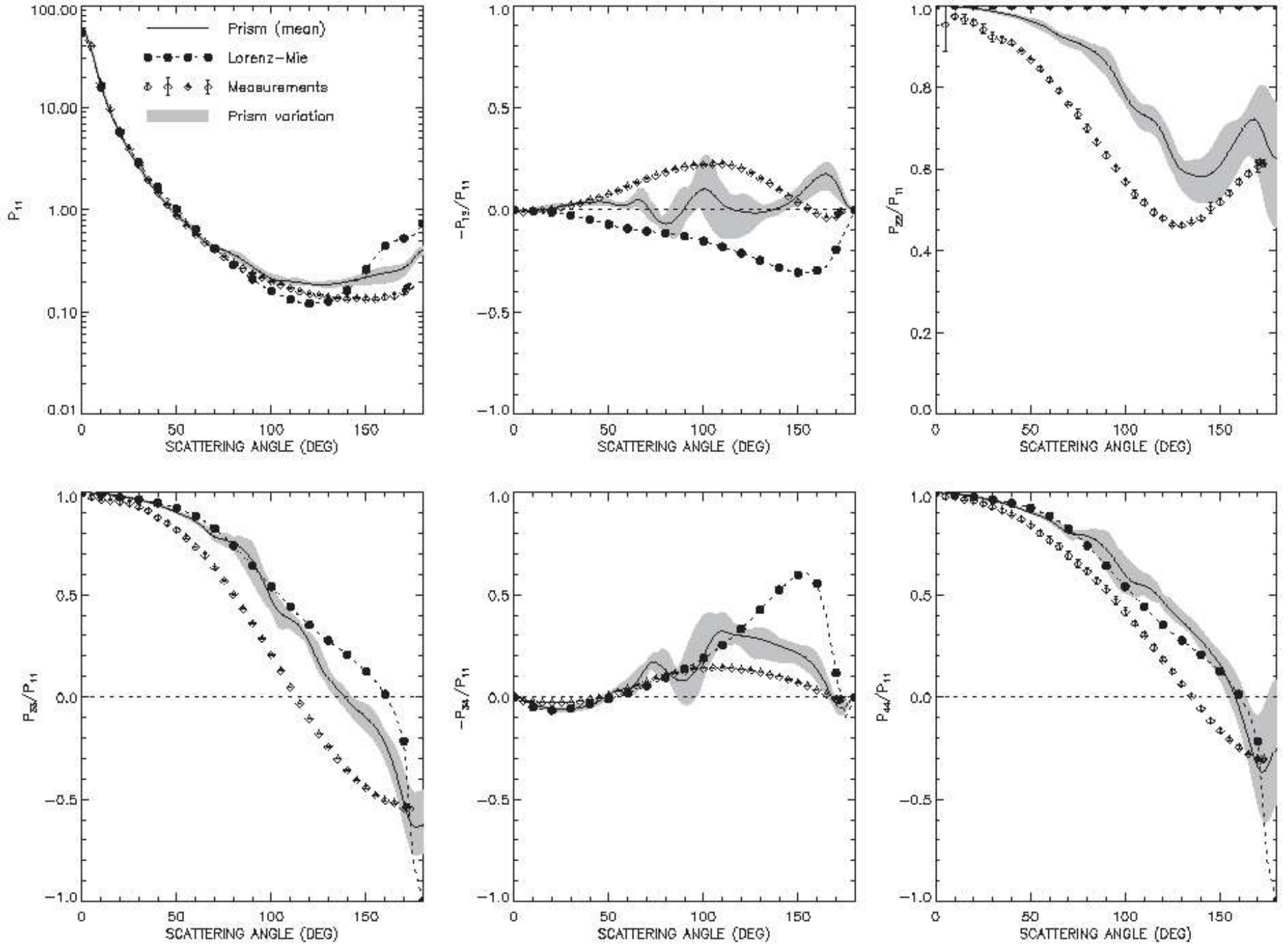

Fig. 2. Comparison of the laboratory measurement with light scattering simulations based on an equi-probable distribution of all 12 different model polyhedral prisms. A Lorenz–Mie solution for perfect spheres is shown for comparison.

TMM applications: cluster of spheres

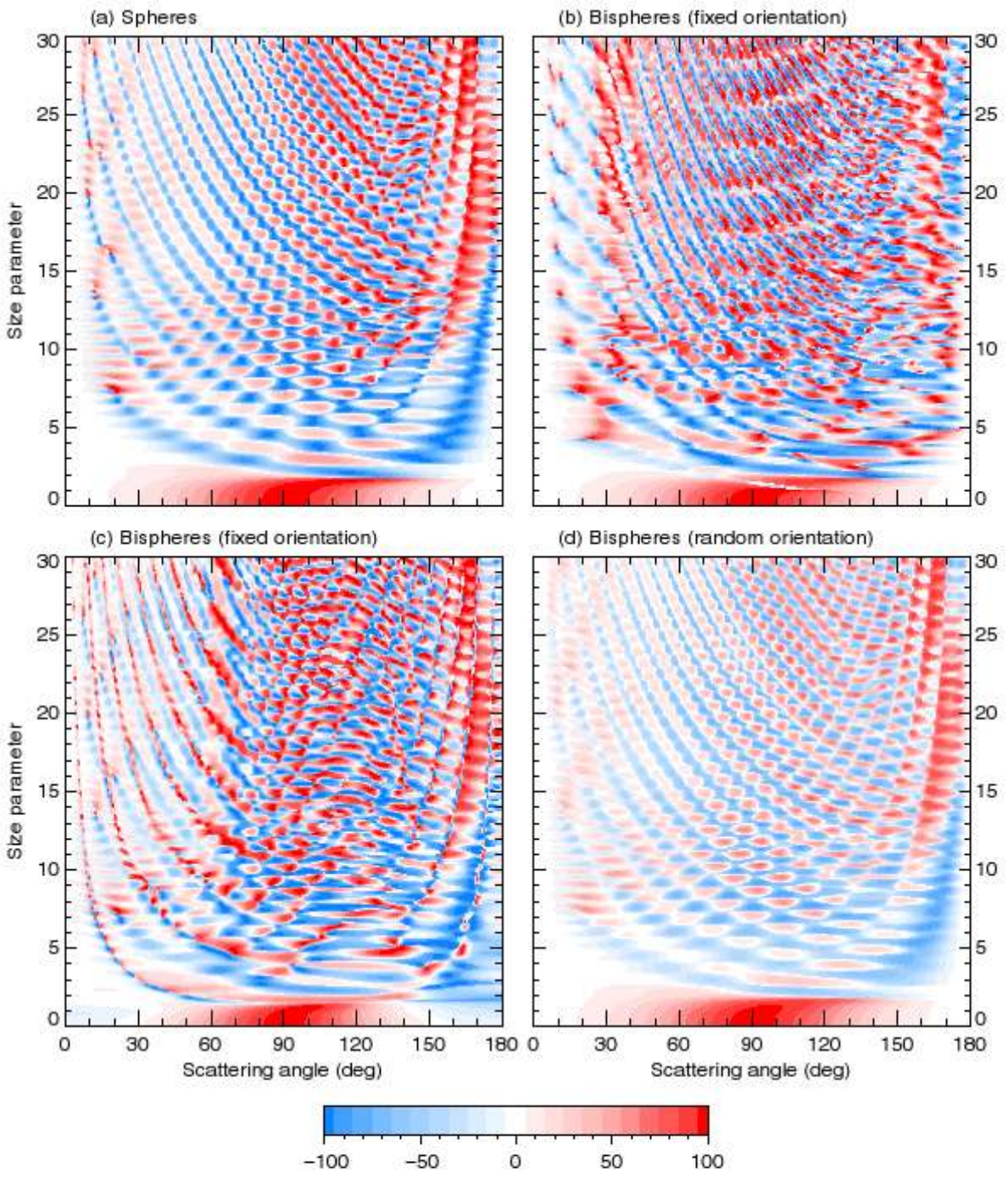

Plate 10.8. Panel (a): the ratio $-Z_{21}(\vartheta^{\rm sca}, \varphi^{\rm sca}=0; \vartheta^{\rm inc}=0, \varphi^{\rm inc}=0)/Z_{11}(\vartheta^{\rm sca}, \varphi^{\rm sca}=0; \vartheta^{\rm inc}=0, \varphi^{\rm inc}=0)$ in % versus $\vartheta^{\rm sca}$ and size parameter for monodisperse single spheres. Panels (b)–(d): the same ratio versus $\vartheta^{\rm sca}$ and constituent-sphere size parameter for monodisperse bispheres with equal touching components in fixed and random orientations. In panels (b) and (c) the bisphere axis is oriented respectively along the z-axis and along the x-axis of the laboratory reference frame. The relative refractive index is $1.5 + i0.005$.

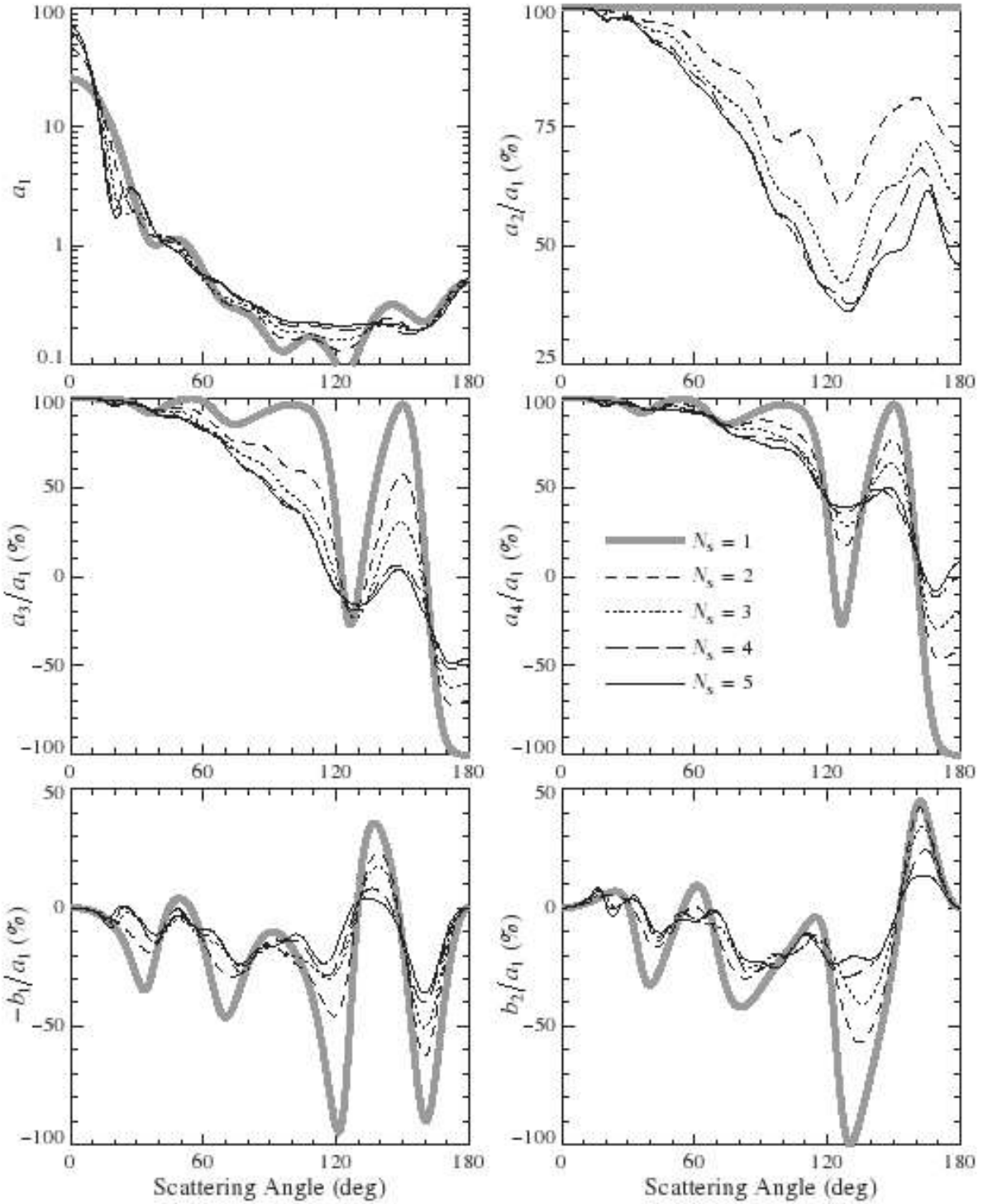

Figure 10.61. As in Fig. 10.60, but for packed clusters of N_s equal spheres. (After Mackowski and Mishchenko 1996.)

Available TMM codes

- Thomas Wriedt: www.t-matrix.de
- Michael Mishchenko:
  http://www.giss.nasa.gov/staff/mmishchenko/t_matrix.html
- Daniel Mackowski:
  http://www.eng.auburn.edu/users/dmckwski/scatcodes/
- Yu-lin Xu: http://www.scattport.org/files/xu/codes.htm